Quasi-optic terahertz imaging

J. O'Hara and D. Grischkowsky

School of Electrical and Computer Engineering and Center for Laser and Photonics Research, Oklahoma State University, Stillwater, Oklahoma 74078

Received May 8, 2001

We demonstrate quasi-optical, diffraction-limited two-dimensional image production by means of reflected pulses of terahertz (THz) radiation. A spherical mirror is used to form a real one-to-one THz image of two 1-mm-diameter steel spheres, which is then scanned over a THz receiver. Diffraction-limited spatial (cross-range) resolution and THz pulse range resolution are simultaneously observed. © 2001 Optical Society of America

OCIS codes: 110.0100, 250.0250.

Imaging with free-space pulses of terahertz (THz) radiation has been demonstrated in many configurations. Many THz images are formed by scanning a sample through a tightly focused THz beam, where either transmitted[1] or reflected[2] radiation is measured. Electro-optic detection techniques have also been used to generate images without scanning of the sample and are excellent for THz beam profiling.[3,4] Spectroscopy, tomography, and beam profiling are just some of the applications of these methods.[4,5]

Using a completely different approach, we demonstrate diffraction-limited THz imaging by using quasi-optic methods in a reflection geometry. In this arrangement, radiation illuminates the entire object, and the resultant image is projected through the system's optics. This complete image is translated in front of the fixed THz receiver, where it is recorded one portion at a time. Except for the generation and reception of the THz radiation, this arrangement uses optical methods exclusively to achieve imaging. Moreover, the THz radiation is pulsed, so this arrangement simultaneously provides a ranging view of the object, similar to those provided by conventional radar systems. Together, these properties make possible three-dimensional imaging of large, nonuniform, and opaque objects.

The quasi-optic THz imaging system, as shown in Fig. 1, is similar to previous THz impulse ranging systems.[6] The key differences are in their methods of THz reception. Figure 1 shows that the transmitted THz beam is slightly focused by a large silicon lens to illuminate the overall object, two 1-mm-diameter steel spheres separated by ~1.4 and ~1.1 mm in the x and z directions, respectively. The frequency-independent $1/e$ amplitude beam diameter of the beam incident upon the object is ~14 mm. The radiation scattered from the object is collected by a 152-mm-diameter spherical mirror with a focal length of 305 mm. The mirror is placed 610 mm from the object (measured along the optic axis) and forms a real, one-to-one (1:1) image, which is also 610 mm from the mirror. The receiver is fixed 627 mm from the mirror, or 17 mm from the image. The image is projected, with a size reduction, onto the receiver's antenna by a hyperhemispherical silicon lens. The antenna is a 50-μm dipole on a silicon-on-sapphire optoelectronic chip similar to those used in many THz systems[7] and is fixed in the image plane of the silicon lens.

Because the system's optic axis is not coincident with the axis of the spherical mirror, it is necessary to ensure that astigmatism will not noticeably degrade the image. Thus the angle θ between the incident and reflected rays of the spherical mirror is only ~10°. At this angle, diffraction limits the resolution ~2.5 times more than does astigmatism. Other relevant aberrations, including spherical aberration and coma, affect the image less than astigmatism and are therefore not major concerns.

The object sits atop a translation stage that allows its position to be controlled. Because of the 1:1 imaging by the spherical mirror, object movements cause equivalent image movements in front of the fixed

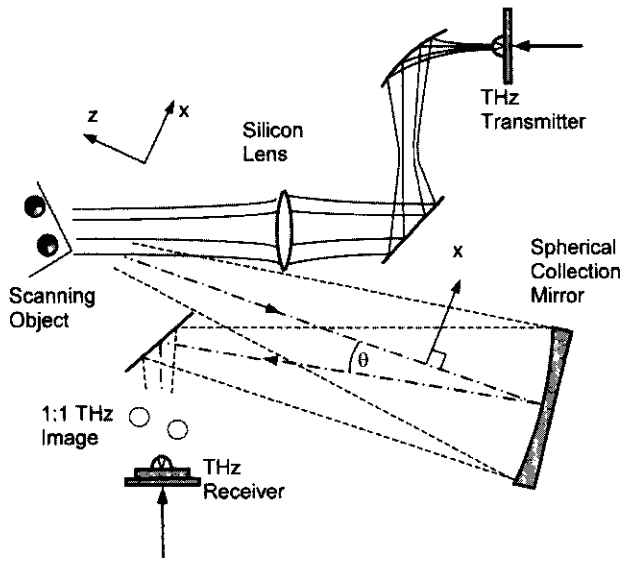

Fig. 1. Quasi-optic THz imaging system. The object, two 1-mm-diameter steel spheres, is placed on a stealth-shaped paraffin holder for invisibility. It is translated in the x direction by a motorized translation stage. The system's optic axis is defined by the dashed–dotted lines.

0146-9592/01/231918-03$15.00/0

receiver. Similarly, the reduced image projected onto the receiver's antenna is translated proportionally. Thus, as the object is translated, the reduced image scans across the receiver antenna.

To make a single measurement (Fig. 2), we fix the object at position x, and the receiver measure the portion of the image within its reception area while the time delay is scanned. The result is a time-domain measurement $E(t,x)$, a current- (in picoamperes) versus-time delay (in picoseconds) measurement. The field amplitude of the received THz radiation is proportional to this measured current. To make all the measurements of Fig. 3, we repeated this process 60 times. For each time-domain measurement, the object was incrementally moved 0.1 mm until the entire 6-mm range was covered. Plotting these time-domain measurements together forms a two-dimensional image of the object. Imaging in three dimensions would simply require an additional object movement in the vertical, or y, direction, resulting in time-domain measurements of the form $E(t,x,y)$.

The resultant fin shapes of the spheres in the image exhibit many features. The orientation of the fins in the image is at an angle to the x axis, which verifies the expected timing changes induced in the system each time the object is moved. Both fins have an ~320-fs temporal width and a 1.76-mm spatial width (FWHM). The stark contrast between these widths is one of the most distinct features of the THz image, showing the resolution benefits of a pulsed system. One can directly translate the temporal dimension (in picoseconds) to the spatial z dimension (in millimeters) by multiplying by 0.15. This conversion constant includes a factor of 2, which accounts for the round-trip distance over which the pulse travels. Figure 4 clarifies the separation of the two spheres in both time and space.

To describe the system in the temporal dimension it is appropriate to adopt the concept of range resolution. With a main pulse width (measured between the zero crossings) of approximately $\tau = 540$ fs, the radar ranging formula[8] $\Delta R = c\tau/2$ yields a spatial z range resolution of $\Delta R = 81$ μm. To calculate the spatial (cross-range) resolution in the x dimension, a different approach is necessary.

Because the object spheres are small, they can be approximated as point sources whose radiation reaching the mirror consists of uniform, diverging spherical waves. Because astigmatism is negligible, it is approximated that the mirror almost perfectly transforms these waves into apertured, uniform, converging spherical waves. At their focus, which lies in the image plane and ~5° off the axis of the mirror, these waves form 1:1 diffraction-limited images of the point sources. These approximated waves can be used for calculating diffraction and overall spatial resolution.

Reference 9 provides a treatment for finding the diffraction-limited amplitude pattern in the vicinity of the geometrical focus of monochromatic, spherical waves converging from a finite aperture. It is noted that, in the plane of the focus (the image plane for our system), the square of the absolute value of the resultant pattern is the familiar Airy intensity pattern for diffraction from a circular aperture.[9] Because the THz imaging system is broadband and coherent in nature, the treatment of Ref. 9 must be extended to a weighted superposition of individual monochromatic, phase-coherent patterns. This superposition of patterns represents the total diffraction-limited image at the focus. With the useful spectrum of the system ranging from 0.2 to 2.5 THz, peaking at 0.7 THz, the calculated, diffraction-limited spatial amplitude image size (FWHM) is 1.79 mm. This gives a spatial (cross-range) resolution of approximately 2 mm at 610 mm, or 3.3 mrad for the broadband THz pulse. These values are consistent with the less-accurate monochromatic Rayleigh resolution criterion of $1.22\lambda/D$, which yields a cross-range resolution of 3.4 mrad at 0.7 THz. The theory is in excellent agreement with the actual data for which the FWHM of the fins measured along the x axis is 1.76 mm.

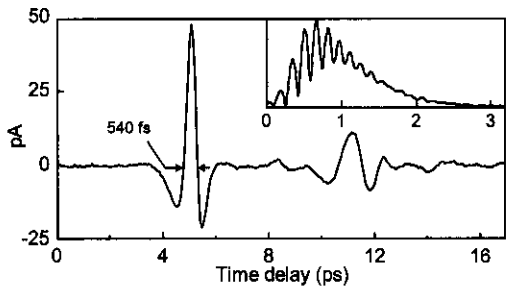

Fig. 2. Single time-domain measurement, $E(t, 2.4$ mm), with its normalized amplitude spectrum shown in the inset. The arrows indicate the pulse width, $\tau = 540$ fs, used for finding the range resolution. The horizontal scale of the spectrum is in units of THz.

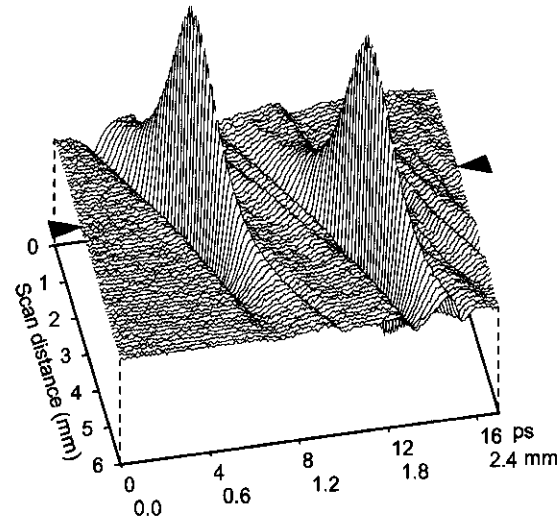

Fig. 3. Two-dimensional image of the object. The image is a composition of 61 individual time-domain measurements represented by contours, each corresponding to a constant value in x. The image shows one temporal and one spatial dimension. We have given two scales for the z axis to show the direct translation of time (in picoseconds) into space (in millimeters). The triangles indicate the location of the individual time-domain measurement, $E(t, 2.4$ mm), shown in Fig. 2.

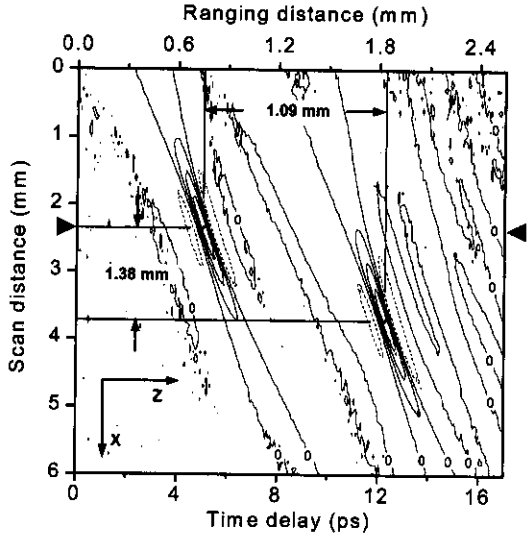

Fig. 4. Contour plan view of Fig. 3. The separation between the spheres is given in both the x and the z directions. The peak amplitude of the image is normalized to unity, and contour lines represent 0.25 steps; therefore contours at 0.50 are the half-maximum contours. Small dots mark the locations of the two peaks. Normalized peak amplitudes are 1 and 0.98 for the left and right peaks, respectively. Zero contours are labeled for reference. Negative contours are shown as dashed curves. The triangles indicate the location of the individual time-domain measurement, $E(t, 2.4\ \text{mm})$, shown in Fig. 2.

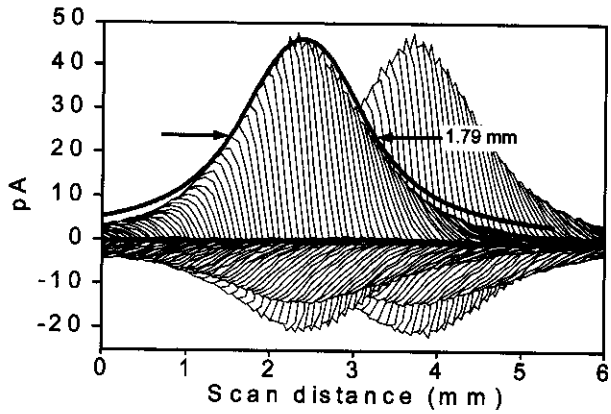

Fig. 5. Direct comparison of theoretical and experimental spatial resolution. The thick curve is the calculated, diffraction-limited spatial amplitude pattern. It is plotted against the two-dimensional image viewed in the z direction. For clarification, the two-dimensional image is plotted as a composition of contours that are constant in z, unlike in Fig. 3 where contours are constant in x. With this view, image features that occur earlier in time obstruct image features that occur later in time. Later features are visible only when their magnitudes exceed those of the earlier features. This view also reveals some of the negative signal data, which, as expected, show the same diffraction effects as the positive signal data. The FWHM of the calculated pattern, 1.79 mm, is indicated by the arrows.

Figure 5 shows the shape of the calculated image and its direct comparison with the experimental results.

We have also observed that a decrease in aperture size of the imaging mirror causes a proportional increase in diffraction-limited image size. When the diameter of the spherical mirror was halved to 76 mm, the measured image size approximately doubled in width, as expected. This proves that the image size was indeed limited by diffraction and not by astigmatic smearing.

The diffraction-limited focal structure of an apertured, converging spherical wave is somewhat tubular in shape, with the highest intensities along the optic axis.[9] This tubular focus is responsible for a significant tolerance in positioning of the receiver plane. We have observed this effect by taking measurements with the receiver fixed at various positions (in a 25-mm range) along the optic axis. Our images were only slightly affected by this motion, thus verifying the tubular shape of the focal region.

In conclusion, reflective quasi-optic THz imaging is a powerful means for investigating independent processes that occur in complex systems such as pulsed radar. Moreover, it promises application in noninvasive imaging arenas for which microwave techniques cannot provide sharp enough resolution and optical techniques cannot be used because of opacity or optical sensitivity. Applications such as burn diagnostics, quality control, tomography, and topography could benefit greatly from such an arrangement.

This research was partially supported by the National Science Foundation and the U.S. Army Research Office. D. Grischkowsky's e-mail address is grischd@ceat.okstate.edu.

References

1. B. B. Hu and M. C. Nuss, Opt. Lett. **20,** 1716 (1995).
2. D. M. Mittleman, S. Hunsche, L. Boivin, and M. C. Nuss, Opt. Lett. **22,** 904 (1997).
3. Q. Wu, T. D. Hewitt, and X.-C. Zhang, Appl. Phys. Lett. **69,** 1026 (1996).
4. Z. Jiang and X.-C. Zhang, Opt. Lett. **23,** 1114 (1998).
5. D. Mittleman, M. Gupta, R. Neelamani, R. Baraniuk, J. Rudd, and M. Koch, Appl. Phys. B **68,** 1085 (1999).
6. R. A. Cheville and D. Grischkowsky, Appl. Phys. Lett. **67,** 1960 (1995).
7. M. van Exter and D. Grischkowsky, IEEE Trans. Microwave Theory Tech. **38,** 1684 (1990).
8. F. Ulaby, *Fundamentals of Applied Electromagnetics* (Prentice-Hall, Englewood Cliffs, N.J., 1997), Sec. 10-5.3.
9. M. Born and E. Wolf, *Principles of Optics*, 7th ed. (Cambridge U. Press, Cambridge, 1999), Secs. 8.8.1 and 8.8.2.